Aerosol Size Distribution using Lidar Data and a Typical Lidar Assembly

HAMED PARSIANI[1] AND JAVIER MÈNDEZ[2]
Department of Electrical and Computer Engineer
University of Puerto Rico, Mayagüez (UPRM) Campus
PO Box 9000, Mayagüez , P.R. 00681-9000
PUERTO RICO
[1]parsiani@ece.uprm.edu [2]javier.mendez2@upr.edu
http://ece.uprm.edu/noaa-crest/

Abstract: - An algorithm is developed and detailed in this paper which determines atmospheric aerosol parameters such as backscatter and extinction coefficients, aerosol optical thickness, and the aerosol size distribution. The algorithm uses the power profile data obtained from Lidar at the City University of New York (CUNY). The aerosol optical thickness at 20 km range has been validated using a Sun-photometer.
The assembly of a typical Lidar system capable of providing the power profile at three standard wavelengths of 355, 532, and 1064 nm is elaborated upon, by actually detailing the Lidar system under construction at the University of Puerto Rico at Mayaguez, as one of several Lidars to be established in the Caribbean.

Key-Words: -Remote sensing, LIDAR system, Aerosol Optical Depth, Aerosol Size Distribution

1 Introduction

The Troposphere aerosols play an important role in the atmospheric process such as the Earth's radiation budget, clouds, precipitation, and air quality. The aerosol study in the Caribbean region is very important, because there are different aerosol types such as: dessert dust, marine, urban, and others.

Light Detection and Ranging (LIDAR), is a system used to sample the atmosphere by analyzing the atmospheric reflection of a transmitted beam of light. The system will be used to characterize the aerosols in the atmosphere above the western part of Puerto Rico. The UPRM LIDAR is being developed with specifications comparable to those of Calipso satellite Lidar, Arecibo Observatory Lidar (AOL) and CUNY LIDARs. The data to be generated by Lidar can be cross validated by Calipso, Sunphotometer (SPM) & AERONET(aerosol network web which reports AOD measurements using a CIMEL with 7 wavelengths).

To characterize aerosol, an algorithm was developed in Matlab. The inversion method presented by Klett and Fernald has been used in this implementation [1, 2] for extinction and backscatter coefficient determination. The ASD was determined using the Lidar inversion method presented by Muller[3] with regularization [4].

2 LIDAR System

The basic block diagram of a Lidar system is shown in Fig. 1, which consists of a transmitter (a laser) a receiver (a telescope), and a detection system, followed by a data acquisition component. The LIDAR System components such as mirrors, lenses, and filters, must satisfy reflectance and transmittance specifications, hence, are carefully selected. Also, to be carefully considered is the power damage threshold of the components directly receiving laser beam.

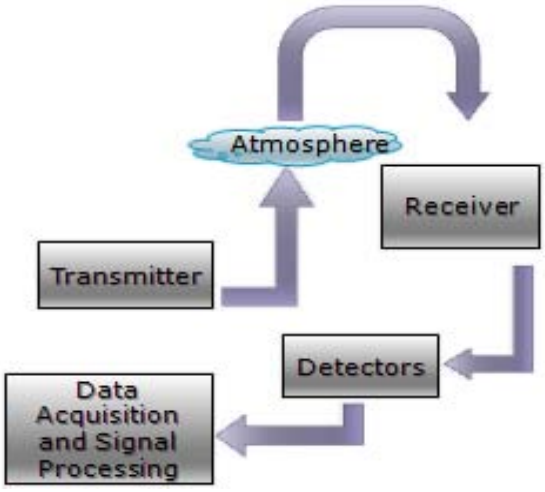

Fig.1 LIDAR system Block diagram

2.1 UPRM Lidar specifications

The UPRM Lidar is a stationary system and the specifications of this system are given by table 1 & 2.

Transmitter			
Laser		*COAR Beam Expander 15.5X9*	
Laser	Brilliant-B Nd: YAG	Input Beam Diameter	9 mm
Wavelengths	1064, 532, 355nm	Output Beam Diameter	140 mm
Energy/Pulse	700mJ at 1064 nm 300mJ at 532nm 120mJ at 355nm	Expansion Ratio	15.5X
		Convex Mirror	Radius = 14.7mm Diameter 25mm Spherical
Pulse period	5ns at 355, 532 and 1064nm	Concave Mirror	Radius =1785mm Diameter 150mm Off-axis segment Ellipsoidal
Frequency	20 Hz	Mirror Separation	835.5 mm

Table 1 UPRM Lidar system transmitter specifications.

Receiver			
UPR 20" F/4 Cassegrain Telescope		Detectors	Hamamatsu
Optical System	Dall-Kirkham Cassegrain	*355nm* *532nm* *1064nm*	PMT: HA9626 PMT: LD0280 APD
Aperture	19.5 inches		
Primary Mirror	F/1.5 Radius=59 inches Concave Ellipsoidal		
Secondary Mirror	Radius=32.3 inches Convex Spherical		
Amplification	2.67 X	Data Acquisition	Licel TR 20-160
Mirror Separation	18.9 inches		
Aperture	19.5 inches		

Table 2 UPRM Lidar system Receiver specifications.

The laser beam departing from the top, Fig. 2, is coaxial with the telescope axis, eliminating the overlap problem between the reflected spot and field of view of the telescope. The very weak beam received from the telescope is focused on a focal point of a lens (f=30 mm) which transmits a parallel beam of diameter 8 mm. The beam is split twice by two bi-directional selectors positioned at 45 degrees to the incident beam, Fig. 2.

The results are three 8 mm beams of wavelengths approximately: $\lambda_1<400$, $400<\lambda_2<900$, and $900<\lambda_3$. These beams after passing through attenuators (if the beam is too strong for the detectors) are submitted to three interference filters which allow only 355, 532, and 1064nm wavelengths to pass. The bandwidth of the first two filters is 3 angstroms and the last one is 3nm.

Three extremely sensitive sensors have been acquired. Two are PMTs (Photo Multiplier Tube) for 355 and 532nm of near 10^6 gain, and one APD (Avalanch PhotoDiode) sensor for 1064nm of near 10^3 gain.

There are three guide mirrors installed at 45 degrees on the exterior of the telescope which guide the laser beam up to the atmosphere, coaxial to the center of the telescope.

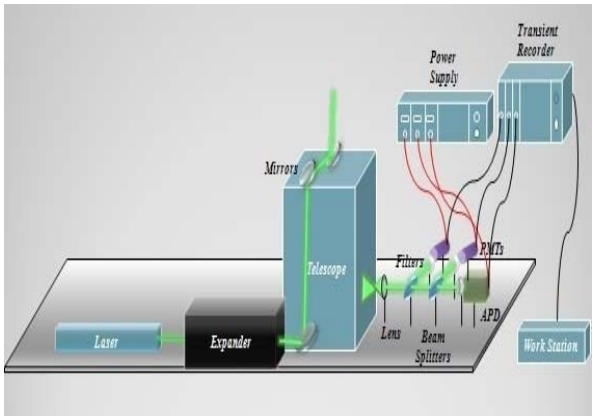

Fig.2 UPRM LIDAR System. It's being developed by the UPRM NOAA CREST LIDAR Division.

3 Aerosol Characterizations

The retrieval of the aerosol optical properties is based on the measurements of the aerosol backscatter and extinction coefficients (β_{aer} and α_{aer}). These coefficients in this paper are determined using CUNY Lidar power profile data at the three fundamental wavelengths. The determination of the vertical profile of the β_{aer} and α_{aer} relies on the LIDAR inversion technique following a far-field inversion algorithm, as proposed by Fernald and Klett, where no multiple scattering corrections are applied, under the assumption of elastic scattering by spherical aerosols. It is well known that multiple scattering occurs mostly under low visibility conditions (presence of water droplets, ice crystals, fog, haze, etc) [1,2].

3.1 Theory

The elastically lidar-returned signal is given by: [3]

$$P(R)=\frac{E_0\eta_0}{R^2}O(R)\beta_T(R)Exp\left[-2\int_0^R\alpha_T(r)dr\right] \quad (1)$$

Where P(R) is the received power at distance R, E_0 is the transmitted power, η_0 is the combined efficiencies of the optical and detection units, O(R) is the overlap between the outgoing laser beam and the receiver field of view (FOV), $\beta_T(R)$ and $\alpha_T(r)$ are the total backscatter and extinction coefficients. The term R^2 in the denominator is for the receiver FOV variations with range.

The total backscatter and extinction coefficients are composed of molecules (Rayleigh) and aerosols (Mie).

$$\beta_T(R)=\beta_{aer}(R)+\beta_{mol}(R) \quad (2)$$

$$\alpha_T(R)=\alpha_{aer}(R)+\alpha_{mol}(R) \quad (3)$$

Where, $\alpha_{mol}(R)$ and $\beta_{mol}(R)$ can be obtained form the best available meteorological data or an approximation from the standard atmosphere. The determination of $\beta_{aer}(R)$ and $\alpha_{aer}(R)$ is more complex. To facilitate this determination, the aerosol lidar ratio (L_{aer}) is assumed to be a constant in most Lidar studies [2].

$$L_{aer}=\frac{\alpha_{aer}(R)}{\beta_{aer}(R)} \quad (4)$$

The L_{aer} can be estimated from other sources, such as data tables, AERONET or Sun-photometer. The solution of the aerosol backscatter is presented in eq. 5 [1].

$$\beta_{aer}(R)+\beta_{mol}(R)=\frac{S(R)Exp\left[-2[L_{aer}-L_{mol}]\int_{R_0}^{R}\beta_{mol}(r)dr\right]}{\frac{S(R_0)}{\beta_{aer}(R_0)+\beta_{mol}(R_0)}-2L_{aer}\int_{R_0}^{R}S(r)Exp\left[(L_{aer}-L_{mol})\int_{R_0}^{r}\beta_{mol}(z)dz\right]dr} \quad (5)$$

Where, S(R) = $P(R)R^2$ is the range corrected received power, R_0 is a reference altitude, and it is chosen to be the highest point in the Lidar range.
This solution fixes the boundary condition at the top of the Lidar range and seeks a solution by back-ward integration that is more stable than the corresponding forward solution [2]. $R > R_0$ is known as forward integration, and if $R < R_0$ then a backward integration is applied [1].

$\alpha_{aer}(R)$ is determined using eq. 4 and the solution of eq. 5. The integration of the total extinction coefficient is known as the Aerosol Optical Thickness (AOT) of the atmosphere, from ground to a desired height. The optical depth is a measure of transparency, and is defined by [5].

$$AOT(R)=\int_0^R\alpha_T(r)dr \quad (6)$$

From eq. 6, the Aerosol Optical Depth (AOD) can be determined at a desired range. The total vertical column AOD can be obtained using a SPM or AERONET station. However, with the SPM and AERONET only a single AOD value is obtained for a column of atmosphere [6].

3.2 Optical Results

The results are obtained using the 355,532 and 1064nm power profiles from CUNY in June 16, 2006 at 1:19 PM. In this research, an algorithm is developed to compute the extinction and backscatter coefficients, and optical thickness. The algorithm uses the standard atmospheric assumptions for molecular extinction and backscatter computation. The aerosol backscatter coefficient, extinction coefficient, and AOT are determined from equations 5,4, and 6 respectively.

Figures 3 and 4 show the aerosol extinction and backscatter coefficients. The spike at 3 and 4km represents a cloud. This is decided based on the assumption that the backscatter coefficient larger than 0.4 represents the presence of cloud [7]. There is a high concentration of aerosols at the 6 to 20km. The aerosols at the first 2 or 3km represent the city fog.

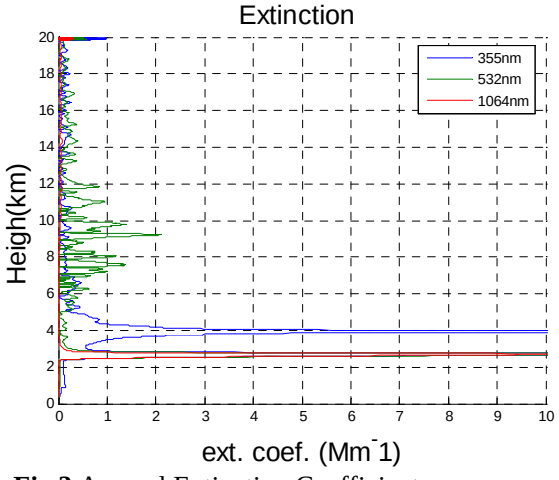

Fig 3 Aerosol Extinction Coefficient.

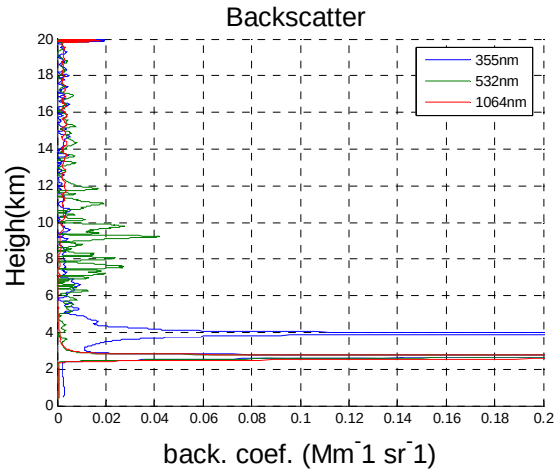

Fig 4 Aerosol Backscatter Coefficient.

Figure 5 shows the AOT at the first 20 km. The AOT plot can provide AOD readings at different atmospheric ranges. For example, the AOD at 20km is 0.3261 for 355nm, 0.2063 for 532nm, and 0.05564 for 1064nm. The AOD at a maximum range obtained from a Lidar can be verified against a nearby SPM or an AERONET station.

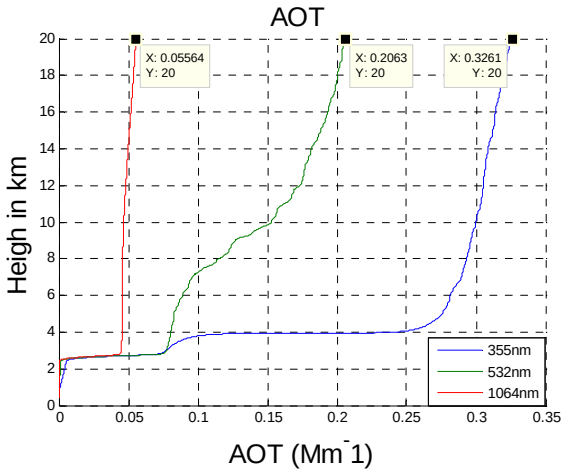

Fig 5 Aerosol Optical Thickness.

The AOT values presented in table 3 are obtained from an AERONET station in CUNY. This table shows the day average values, but it does not include the three fundamental Lidar wavelengths. For this reason the desired AOT at the desired wavelengths has been interpolated. Table 4 shows the complete chart with the interpolated values for the desired wavelengths.

Comparing the values obtained at 20km using the Lidar profiles (Fig. 4) and the interpolated values in table 4, we see that the values are very close. The following error percentages are obtained in this comparison: **7.6% at 355nm**, **4.7% at 532nm**, and **3% at 1064nm**. This comparison demonstrates that at high altitudes the Lidar AOT measurements coincide well with the AOT readings by an AERONET station or a portable Sun-photometer (SPM). The AOT is typically smaller for longer wavelengths than for shorter wavelengths. Also see [8].

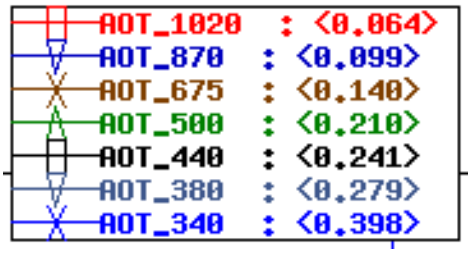

Table 3 CIMEL (AERONET station) average AOD values in CUNY at June 16, 2006.

AOT_1064	0.054
AOT_1020	0.064
AOT_870	0.099
AOT_675	0.140
AOT_532	0.197
AOT_500	0.210
AOT_440	0.241
AOT_380	0.279
AOT_355	0.353
AOT_340	0.398

Table 4 Interpolated values for 355, 532 and 1064nm.

4 Aerosol Size Distribution (ASD)

The range of the actual size distribution for atmospheric aerosols varies from approximately 50nm to 15 μm radius. Aerosols that are found in the atmosphere are not always spherical. In this paper aerosols are assumed to have spherical shapes[9].

The ASD for a column of atmosphere could be determined using instruments such as the SPM and AERONET. However, ARONET provides a single ASD for a vertical column of atmosphere. Whereas, Lidar provides a comprehensive ASD profile which represents ASDs at different heights. The ASD can

be obtained from the backscatter and extinction coefficients at a specific altitude. The inversion method implemented is Tikhonov's with regularization. This methodology is implemented using the optical data at the three fundamental wavelengths (355, 532 and 1064nm). It is possible to validate ASD with in-situ Sun-photometer data, but as shown in [6], it requires a Neural Network to take the SPM data and convert it to ASD data after it has been trained with AERONET data. The Neural Network application could be simply done by using MatLab Neural Network tool box as can be seen implemented, as an example, by [10,11].

4.1 Theory

The relationship between the backscatter and extinction coefficients with the volume size distribution of spherical particles can be obtained by eq. 7 [3,12,13]. This equation is known as Fredholm equation.

$$g_p = \int_{r\min}^{r\max} k_p(r,m)v(r)\,dr + e_p^{\exp} \quad (7)$$

Where, g_p represent the optical data such as extinction or backscatter, the subscript p being the number of available optical coefficient at the specific range and wavelength. The term V(r) represents the volume size distribution. k_p is the kernel function for the specific data type. k_p depends on the Mie-efficiencies for spherical particles, the refractive index m, and the radius r [13] (see appendix A). The refractive index is a complex number, where the imaginary part represents absorption. $e_p^{\exp}$ is the equivalent experimental error at the specific optical data.

Volume size distribution $v(r)$ in eq. 7 is typically modeled by logarithmic normal or binomial density function which itself is approximated by a linear combination of B-spline functions $B_j(r)$, of the first type, Eq. 8, where w_j [3] are the coefficients, and e^{math} is the mathematical error due to the approximation.

$$v(r) = \sum_j w_j B_j(r) + e^{math}(r) \quad (8)$$

By substituting $v(r)$ into eq. 7, swapping the integration and summation eq. 10 is formed.

$$g_p = \sum_{j=1}^{n=6} W_j \int_{r\min}^{r\max} k_p(r,m)B_j(r)dr + e \quad (10)$$

The part inside of the integration in eq. 10 represents the weight matrix.

$$A_{pj}(m) = \int_{r\min}^{r\max} k_p(r,m)B_j(r)\ dr \quad (11)$$

Substituting in eq. 10 the A_{pj} integral, and changing it into a matrix form will result in equation $g = Aw + e$. g is the optical data, A=[A_{pj}] is a weight matrix, W=[w_j], and ***e*** is the combined errors.

w_j can be obtained from $g = Aw + e$ by Eq. 12, which presents the solution for a square matrix A :

$$w = A^{-1} g_p \quad (12)$$

Regularization [Appendix C] will be used for smoothening of the errors in the calculations of the coefficients of the B-spline functions. Eq. 13 represents the weights solution with regularization.

$$w = (A^T A + \gamma H)^{-1} A^T g_p \quad (13)$$

Where, γ denotes the Lagrange multiplier, H is smoothing matrix, and g_p is the optical data.

4.2 Results

The kernel functions are computed for spherical particles according to the Mie-theory. Figures 6 and 7 show the backscatter and extinction kernels function for the three fundamental wavelengths. The refractive index plays an important role in the ASD determination. The refractive index depends on the aerosol type. The aerosols are classified into three classes of Urban & Industrial (I), Biomass Burning (II), and dessert dust & Oceanic (III). The refractive index values for each class are given in table 2 [14].

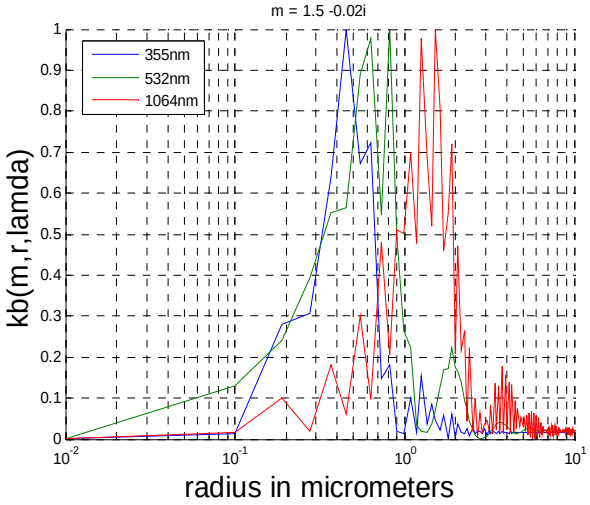

Fig. 6 Normalized backscatter kernel functions.

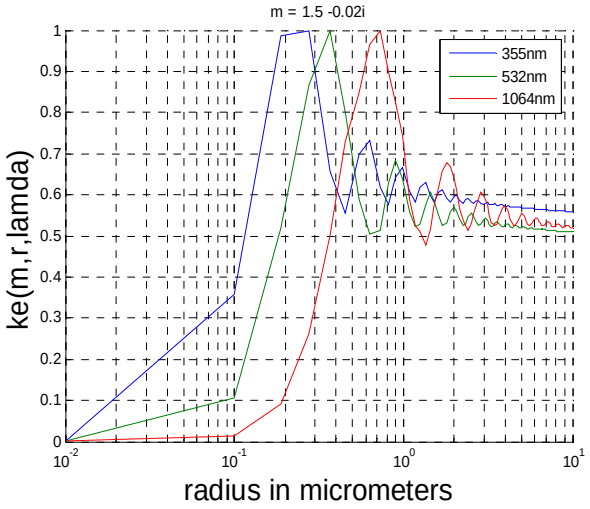

Fig. 7 Normalized extinction kernel functions.

Refractive Index	Urban Industrial I	Biomass Burning II	Dessert dust and Oceanic III
m real	1.4–1.47	1.47–1.52	1.36–1.56
m imag.	0.003–0.015	0.015–0.02	0.0015–0.003

Table 2 Typical refractive index values for different aerosol types.

In this paper the ASD is calculated for a height of 1km. The ASD simulations were presented for the optical characterization of 3β+3α, which implies that the optical data used for volume size determination consists of the backscatter and the extinction coefficients [16].

The Figures 8, 9 ,and 10 depict the volume size distribution for the three types of aerosols as a function of radius measured in the range of .5 to 15 micrometer, presented for data at the 4 Km of atmosphere. Types I and III aerosols are approximated by a monomial distribution, whereas type II aerosol is approximated by a binomial distribution since there isn't enough aerosol of type II at this altitude to justify a monomial distribution function.

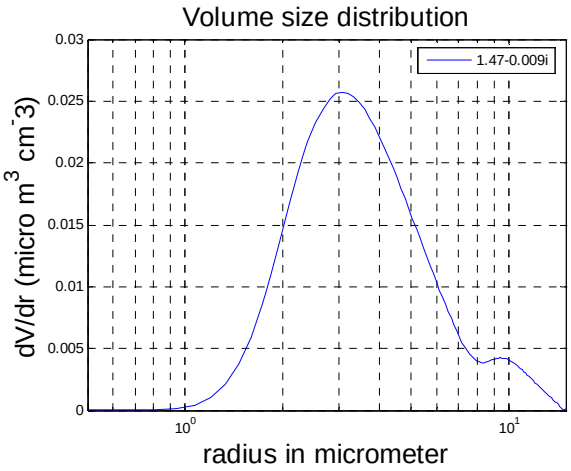

Fig, 8 Retrieval volume size distribution for type I aerosols. Show urban and industrial aerosols presence at 4 km of altitude.

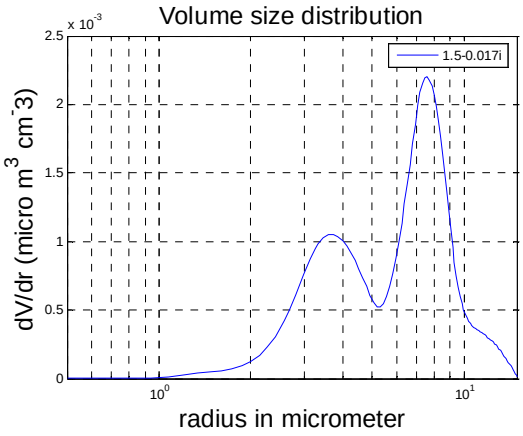

Fig, 9 Retrieval volume size distribution for type II aerosols. Show biomass and burning aerosols presence at radii at 4 km of altitude.

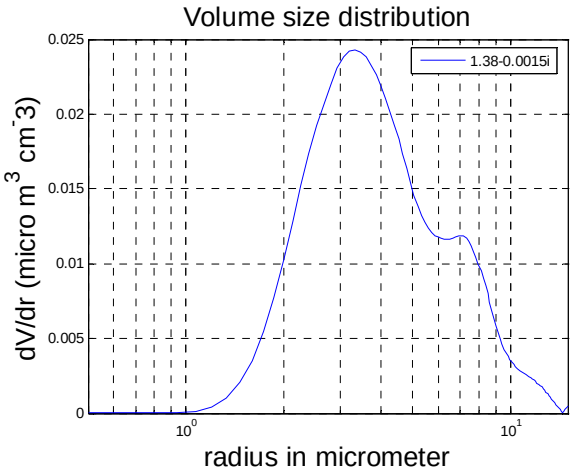

Fig, 10 Retrieval volume size distribution for type III aerosols. Oceanic aerosols present at 4 km of altitude.

The results in figs. 8 to 10 coincide with the atmospheric conditions in New York City (NYC). The high concentration of Urban & Industrial aerosol can be observed in fig. 8, which is reasonable for NYC. The presence of Oceanic aerosols, fig. 9, is also common in the NYC atmosphere due to its proximity to the Atlantic Ocean. On the other hand as shown by fig. 10, the Burning & Biomass aerosols (type III) volume is approximately 10 times less than the other two types, understandably so in NYC atmosphere. The small amount of type III present in the atmosphere is transported from other regions. Table 3 presents the statistics of the obtained results.

	Type I	**Type II**	**Type III**
mean	$8.3\text{x}10^{-3}$	$7.44\text{x}10^{-4}$	$5.8\text{x}10^{-3}$
stdev	$8.2\text{x}10^{-3}$	$7.18\text{x}10^{-4}$	$7.2\text{x}10^{-3}$

Table 3 Basic statistics of the ASD results.

4.3 Effect of regularization on the ASD plots

The smoothness of the plots obtained in figs. 8 to 10 is obtained by the application of the Tikhonov's regularization method as applied to eq. 13, see Appendix C. Figures 11 to 13 present the effect of the regularization, where blue and green plots show the effects with and without regularization, respectively.

Types I & III aerosols have the best approximation in comparison with aerosol type II, due to the very large concentration of the former types in the atmosphere.

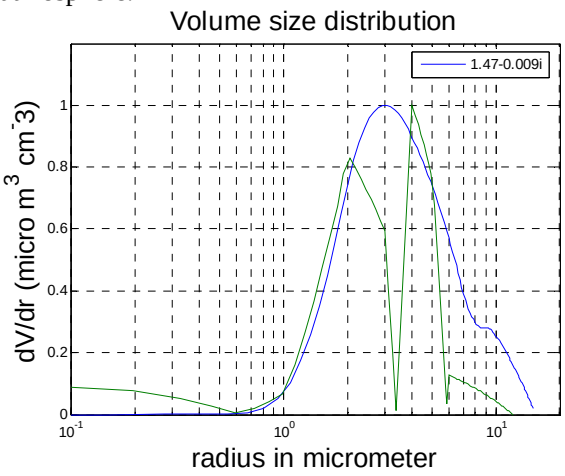

Fig. 11 Aerosols **type I** distribution reconstruction.

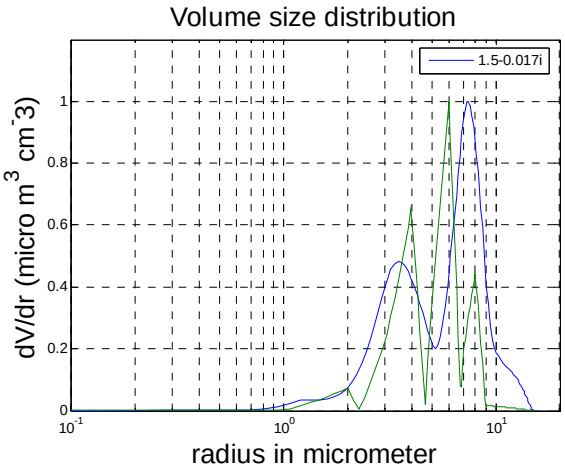

Fig. 12 Aerosol **type II** distribution reconstruction.

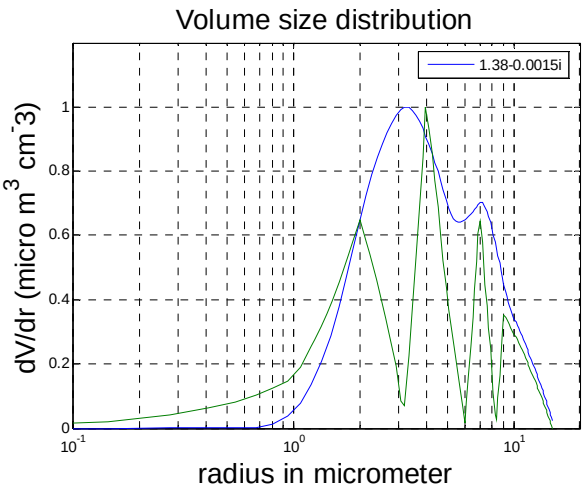

Fig.13 Aerosol **type III** distribution reconstruction.

5 Conclusion

The results are based on the power profile data for three wavelengths of 355, 532, and 1064nm obtained from CUNY Lidar on June 16, 2006. An algorithm was developed for aerosol characterization calculating fundamental parameters such as particle backscatter and extinction coefficients, AOT, and ASD. The ASD determination is based on Muller's algorithm using Tikhonov's inversion with regularization methods.

The results of backscatter and extinction coefficients obtained by the algorithm developed in this research project were validated using AOT results. That is, the AOT values obtained from Lidar data compared favorably with the CIMEL (AERONET station) in CCNY using the average values of the day.

The Aerosol Size Distribution data obtained on a daily basis is fundamental for the improvement of the regional atmospheric model predictions.

The ASD are represented by a monomial and binomial distributions. The distribution depends on the aerosol type existence in the different atmospheric layers.

6 Future work

The UPRM Lidar data will be used to validate CALIPSO Lidar data which has a trajectory passing close to UPRM Lidar . It will contribute to the aerosol characterization over Puerto Rico and the Caribbean.

The ASD data obtained from Lidar power profile at total atmospheric column will be validated using a simpler ASD determination method. This will require access to SPM and the AERONET station data.

Acknowledgements

- Supported by NOAA CREST under grant NA17AE1625 and partially supported by NASA-EPSCOR, NASA-PASSER, and UPRM.
- Special Thanks to:
  Barry Gross, Yonghua Wu, Benjamin Herman and CUNY Lidar Lab staff for supplying the three-wavelengths data, and other documentation. Vazjier Rosario help with the UPRM Lidar system specifications.

References:

[1] James D. Klett, "Stable Analytical Inversion Solution for Processing Lidar Returns," Optical Society of America, Applied Optics/Vol. 20, No. 2/ Applied Optics/ 15 January 1981

[2] Federick G. Fernald, "Analysis of Atmospheric Lidar Observations," Optical Society of America, Applied Optics/Vol. 23, No. 5/1 March1984.

[3] D. Müller, U. Wandinger, and A. Ansmann, "Microphysical Particle Parameters from Extinction and Backscatter Lidar Data by Inversion with Regularization: Theory," *Appl. Opt.* **38**, 2346-2357 (1999).

[4] S. Twomey, "Introduction to the Mathematics of Inversion in Remote Sensing and Indirect Measurements" (Elsevier, 1977).

[5] Ricardo Vergaz Benito, "Atmospheric Aerosol Characterization," Óptica Pura y Aplicada – Vol. 34/ 2001.

[6] Hamed Parsiani, Andres Bonilla, "Aerosol Size Distribution Estimation using Sun photometer and Artificial Neural Network," 12th **WSEAS** International Conference on SYSTEMS, Heraklion, Greece, July 22-24, 2008.

[7] CALIOP Algorithm Theoretical Basis Document Part 2: Feature Detection and Layer Properties Algorithms, 2006.

[8] C. F. Bohren, D.R. Huffman: " Absorption and scattering of Light by small Particles," Wiley, New York, 1983.

[9] Albert Ansmann and Detlef Müller, "Lidar and Atmospheric Aerosol Particles," Optical Sciences, 2005.

[10] YELDA OZEL , IRFAN GUNEY , EMIN ARCA, "Neural Network Solution to the Cogeneration System by Using Coal," 12th **WSEAS** International Conference on CIRCUITS, Heraklion, Greece, July 22-24, 2008.

[11] MAJA SAREVSKA, ABDEL-BADEEH M. SALEM, NIKOS MASTORAKIS, "Null Steering Beamformer Based on RBF Neural Networks," 12th **WSEAS** International Conference on COMMUNICATIONS, Heraklion, Greece, July 23-25, 2008.

[12] Christine Bockmann, "Hybrid regularization method for the ill-posed inversion of multiwavelength lidar data in the retrieval of aerosol size distributions," 2001 Optical Society of America

[13] Pi-Huan Wang, Geoffrey S. Kent, M. Patrick McCormick, Larry W. Thomason, and Glenn K. Yue, "Retrieval analysis of aerosol-size distribution with simulated extinction measurements at SAGE III wavelengths," 20 January 1996 / Vol. 35, No. 3 / APPLIED OPTICS.

[14] Whitby, K. T., R. B. Husar, B. Y. H. Liu, "The Aerosol Distribution of Los Angeles Smog," Journal of Celluloid and Interface Science, Vol. 39, No.1, pp. 177-204, 1973.

[15]N. Larsen, B. Knudsen, T.S. Jorgensen, A. Disarra, D. Fua, P. Digirolamo, G. Fiocco, M.Cacciani, J.M. Rosen, N.T. Kjome, "Backscatter measurements of stratospheric aerosolsat Thule during January-February 1992." *Geophysical Research Letters* **21**, 1303-1306 (1994).

[16] Michael D. King, Dale M. Byrne, Benjamin M. Herman and John A. Regan, "Aerosol Size Distributions Obtained by Inversion of Spectral Optical Depth Measurements," *The University of Arizona, Tucson 85721* (Manuscript received 17 February 1978, in final form 15 August 1978).

[17] C. F. Bohren and D. R. Huffman, "Absorption and scattering of light by small particles", pp. 135-136, (Wiley, New York, 1983)

[18]Markus Pahlow, Detlef Müller, Matthias Tesche, Heike Eichler, Graham Feingold, Wynn L. Eberhard, and Ya-Fang Cheng, "Retrieval of aerosol properties from combined multiwavelength lidar and sunphotometer measurements ," 1 October 2006 _ Vol. 45, No. 28 _ APPLIED OPTICS.

[19] D. Müller, U. Wandinger, D. Althausen, and M. Fiebig,"Comprehensive particle characterization from 3-wavelength Raman lidar observations: case study," Appl. Opt. **40,** 4863–4869(2001).

8 Appendices

Appendix A: Kernel function

The kernel function depends on the Mie efficiencies for spherical shapes. The efficiencies depend on the refractive index n, the wavelength λ, and the particles radii r. The refractive index is a complex number where the imaginary part means absorption. The Extinction efficiency is the sum of scattering and absorption efficiencies. Eq. 14 and 15 show the scattering and absorption efficiencies [17].

$$Q_{sca} = \frac{128\pi^4 r^4}{3\lambda^4}\left|\frac{n^2-1}{n^2+2}\right|^2 \qquad (14)$$

$$Q_{abs} = \frac{8\pi r}{\lambda}\mathrm{Im}\left\{\frac{n^2-1}{n^2+2}\right\}\left[1-\frac{32\pi^3 r^3}{\lambda^3}\mathrm{Im}\left\{\frac{n^2-1}{n^2+2}\right\}^2\right] \qquad (15)$$

The backscatter efficiency is given by eq. 16.

$$Q_{\text{back.}} = \frac{64\pi^4 r^4}{\lambda^4}\left|\frac{n^2-1}{n^2+2}\right|^2 \qquad (16)$$

Finally, The kernel function can be calculated in terms of surface area (Eq. 17) or volume concentration (Eq. 18) [8], where the subscript i represents either of the two data types (extinction or backscatter) at the specific wavelength.

$$K_S = \pi r^2 Q_i \qquad (17)$$

$$K_V = \frac{3Q_i}{4r} \qquad (18)$$

Appendix B: B-Spline Modeling

In this research, base functions are used to stabilize the inversion process. The B-splines functions used are of first degree equidistant triangles. This function permits easy reconstruction of the volume size distribution for monomial and binomial distributions [3]. In this case each B-spline (triangle) has 113 data points. The six B-splines presented in fig. 13 are fixes in a 6x113 array.

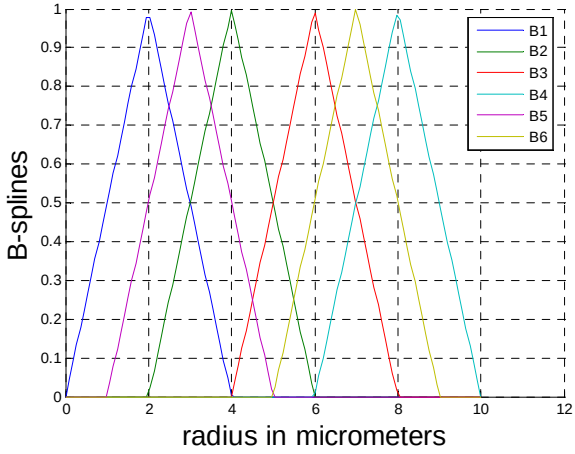

Fig. 13 First order B-splines results.

Appendix C: Regularization Method

The simplest solution of w presented in eq. 12 does not provide restorable results, because it is highly oscillatory. The oscillation provides errors in the solution of the microphysical properties even though the optical data can be reproduced with

high accuracies [4,18,19]. The error e introduced in $g = Aw + e$ is needed to determine the microphysical properties. This is because it is not possible to reproduce the exact optical data [18]. The method of maximum distance defined by Euclidian norm has been applied to the error which is presented by eq. 19.

$$e^2 \geq \|Aw - g\|^2 + \gamma\Gamma(v) \qquad (19)$$

The constraint of smoothness is included in the nonnegative scalar $\Gamma(v)$, and it can be written as [14]:

$$\Gamma(v) = w^T H w \qquad (20)$$

. The eq. 20 measures the deviation of the inverted particle size distribution v(r) from the requested smoothness [18]. The smoothness is the second derivative of the reconstructed particle size distribution. The mathematical formulation of the smoothing matrix H is obtained in eq. 21 [16].

$$H = \begin{bmatrix} 1 & -2 & 1 & 0 & 0 & 0 \\ -2 & 5 & -4 & 1 & 0 & 0 \\ 1 & -4 & 6 & -4 & 1 & 0 \\ 0 & 1 & -4 & 6 & -4 & 1 \\ 0 & 0 & -2 & 5 & -4 & 1 \\ 0 & 0 & 0 & 1 & -2 & 1 \end{bmatrix} \qquad (21)$$

The solution of the minimization concept is obtained through substituting eq. 20 in eq. 19. The solution of the weights factors is given by eq. 13. The scalar γ is the Lagrange multiplier. It varies from a low value to a high value. With γ=0, no smoothing can take place, and the solution of w is given by eq. 12, namely the oscillation effect remains. For high values of γ, the solution is over smoothed, and the second order derivative matrix H can not help in the determination of the model for ASD plot. γ must be chosen such that the eq. 19, becomes a minimum [18].

Appendix D: Aerosol size distribution algorithm

The algorithm developed in this research for the calculation of ASD uses a flow chart as depicted in fig. 14. In this algorithm, the B-spline function matrix is of size 6x113, Kernel matrix k = 6x113, where there are 3β+3α optical data, and a radius vector of 113 different sizes. Matrix A which is determined by eq. 11, and W determined by eq. 11 are of sizes 6x6 and 1x6, respectively. And the final result, volume size distribution of eq. 8, is of size 1x113.

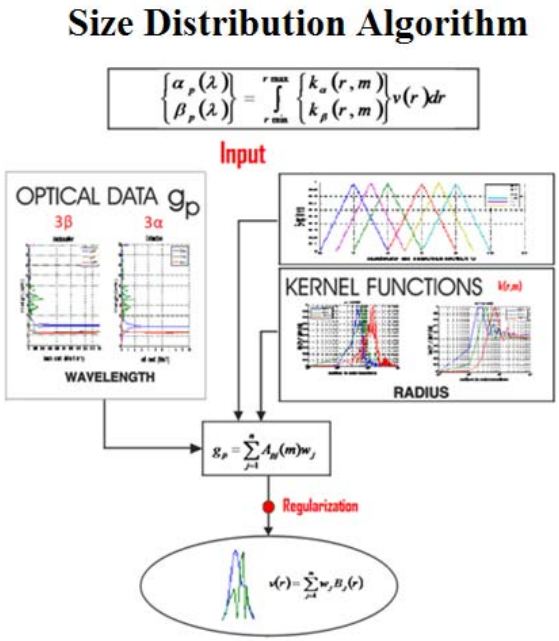

Fig. 14 ASD algorithm block diagram.